Available online at www.sciencedirect.com

ScienceDirect

Procedia CIRP 75 (2018) 214–219

www.elsevier.com/locate/procedia

15th CIRP Conference on Computer Aided Tolerancing – CIRP CAT 2018

Generating T-Maps with the kinematic transformation to model manufacturing variations of parts with position tolerancing of cylinders

Aniket Chitale[a], Nathan J. Kalish[a], Joseph K. Davidson[a]*, Jami J. Shah[b]

[a]*Department of Mechanical and Aerospace Engineering, Arizona State University, Tempe AZ 85287, USA*
[b]*Department of Mechanical and Aerospace Engineering, Ohio State University, Columbus OH 43210, USA*

* Corresponding author. Tel.: +1-480-965-3824; fax: +1-480-727-9321. *E-mail address:* j.davidson@asu.edu

Abstract

The kinematic transformation is used to form part-level T-Maps for patterns of holes from a generic T-Map primitive constructed in a generic coordinate frame at one end of the axis at one hole. The generic T-Map primitive is formed with higher dimensional half-spaces, all arranged tangent to the circular constraint at the one end of the tolerance-zone for the axis. After transforming each of these to a local frame, suitable for the entire pattern, they are intersected to form the part-level T-Map for the entire pattern of holes. The T-Maps are applied to several patterns of cylinders.

Peer-review under responsibility of the Scientific Committee of the 15th CIRP Conference on Computer Aided Tolerancing - CIRP CAT 2018.

Keywords: Modeling geometric deviations; Variation simulation; Kinematic transformation

1. Introduction and purpose

Patterns are arrays of features of size having the same dimensions, tolerancing method and tolerance values. A pattern may be linear, such as the set of openings for electrical contacts in the connector for an Ethernet network cable; circular, such as the array of bolt-holes around a pipe flange; rectangular; or irregular, such as the array of holes for bolting together two halves of the casing for a centrifugal pump. Position control of each feature in the pattern may be accomplished with one tolerance in a single feature control frame or with two control frames (called position tolerancing [1]), each containing a different tolerance. One tolerance (*Pattern-Location Tolerance Zone Frame* (PLTZF)) locates the entire pattern relative to the same datum reference frame (DRF), and the other (*Feature Relating Tolerance Zone Frame* (FRTZF)) controls the location and orientation of features within the pattern. This method is often used for features used to assemble large parts. Ameta, *et al*. [2] illustrated how assembly-level T-Maps represent the distinctions between the three ways, listed in [1], of specifying the PLTZF and the FRTZF. The different T-Maps were generated intuitively. They then used these results to form the first T-Map that mathematically models part-level variations between two parts that are joined by a linear pattern of engaged pins and holes.

In this paper we use the single position tolerance which controls the position of every feature in the pattern relative to the same datum reference frame (DRF). We also apply more general mathematical tools, an adapted form of the kinematic transformation and intersection of higher dimensional half-spaces, to construct the T-Map for *any* pattern of cylindrical features.

2. Specifications and tolerance-zone boundaries

A square pattern of holes is shown in Fig. 1 with basic (theoretical) dimensions that locate holes relative to Datums A, B, and C. The specified tolerance on position (t=0.2 mm) defines the long and slender tolerance-zone at each hole which is centered at its theoretical location (Figs. 2(a) and (b)).

When Part 2 is assembled with a companion Part 1 (Fig. 2(c)) that contains an engaging pattern of four pins, clearances

2212-8271 © 2018 The Authors. Published by Elsevier B.V.
Peer-review under responsibility of the Scientific Committee of the 15th CIRP Conference on Computer Aided Tolerancing - CIRP CAT 2018.
10.1016/j.procir.2018.04.053

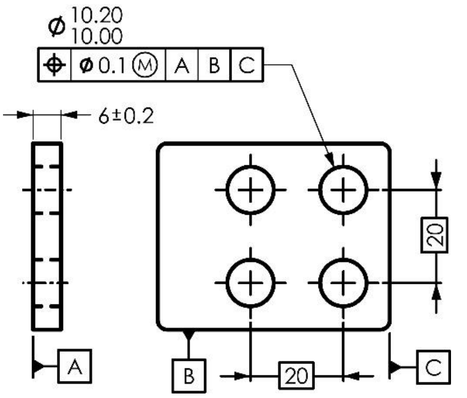

Fig. 1. Specifications for the pattern of holes in Part 2 of Fig. 2(c).

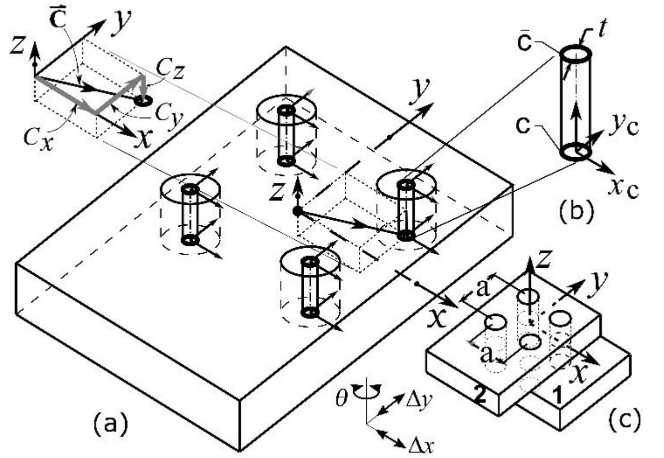

Fig. 2. (a) pattern of four holes, their axis tolerance-zones, and eight constraint circles; (b) two constraint circles for one tolerance-zone; (c) assembled parts 1 and 2.

and manufacturing variations in the holes and pins allow some variation in the relative location of the two parts. We assume that the size limits and position tolerances on the pins and holes of Parts 1 and 2 allow the mating planar surfaces (A) to remain in contact for all allowable variations. Consequently, part-level T-Maps presented in this paper model the limits to variations θ, Δx, and Δy (Fig. 2(c)). Unlike in [2], in this paper we use the single position tolerance which controls the position of every hole in the pattern relative to the same datum reference frame (DRF) [1,3]. The DRF ABC in Fig. 1 is formed with the 3-2-1 principle: (a) three target points of support form Datum A; (b) with these remaining in contact, two additional target points form Datum B; and (c) while maintaining all these five contacts, a single sixth target forms Datum C.

When constructing T-Maps in §§5.3, 6, and 7, we assume that variations arise from tolerances on the holes only, i.e. all pins in an engaging pattern are located theoretically and are made at their virtual condition (VC) size. Then, in §8 we include the effect of tolerances specified for the pins that are located on Part 1 (Fig. 2(c)).

3. T- Maps, deviation spaces, and SDT coordinates for patterns of holes

A Tolerance-Map® (T-Map®) for any feature [4,5] is a hypothetical Euclidean point-space, the dimensions, shape, and internal subsets of which represent all the tolerances on a feature and which limit, according to a designer's intent, its geometric variations when it is manufactured. Although the methods of construction are often different, *deviation spaces* [6] are typically of the same shape for many features. For plane- and line-features, a distinction is that the coordinate labels are different. T-Map coordinates are the classical coordinates for planes and Plücker coordinates for lines [7,8], while the coordinates for deviation spaces are those for the small displacement torsor (SDT) [9,10,11] that represents the small displacements, or freedoms, of a feature relative to a rigid body. Both T-Maps and deviation spaces are orthonormal spaces, i.e. the coordinate axes are pairwise orthogonal. Both also have the same kinematic interpretation: each point of the hypothetical space (the co-domain) corresponds to a unique small displacement of the perfect-form feature within its tolerance-zone. In this paper we use SDT coordinates since the kinematic transformation [5,12] applies to these coordinates directly [13].

Teissandier, *et al.* [14,15] build n-dimensional deviation spaces (polytopes), especially for features having parallel supports, by intersecting sets of half-spaces, each of which models one constraint of the feature. We also use half-spaces in this paper since the intersection of transformed generic T-Maps is central to our method. However, before intersecting them, we transform them with the kinematic transformation, especially adapted to half- spaces and circular constraints [16].

For any feature in its tolerance-zone, the 6D SDT coordinates $(\phi, \psi, \theta; \Delta x, \Delta y, \Delta z)$ represent its small *positive* (CCW) rotations about, and small *positive* translations along, the 3D coordinate x-, y-, and z-axes of the tolerance-zone [9,10,11], such as the xyz-frame in Fig. 2(a).

4. The inverse kinematic transformation for hyperplanes.

Before intersection, each generic T-Map must be transformed from its constraint circle (C) $x_C y_C z_C$-frame (e.g. Figs. 2(b) and 3(a)) to a local (ℓ) frame of reference for the entire pattern. From robotics and kinematics [12,17], the transformation of a six-component small displacement torsor (SDT) $[\phi \ldots \Delta z]^{\mathrm{T}}$ from the C-frame to ℓ-frame is made with the 6×6 general kinematic transformation

$$ {}^{\ell}\begin{bmatrix} \phi \\ \vdots \\ \Delta z \end{bmatrix} = {}^{\ell}\begin{bmatrix} [\mathbf{R}] & [\emptyset_3] \\ [\mathbf{X}][\mathbf{R}] & [\mathbf{R}] \end{bmatrix} {}^{C}\begin{bmatrix} \phi \\ \vdots \\ \Delta z \end{bmatrix} \equiv {}^{\ell}[\$\$] \; {}^{C}\begin{bmatrix} \phi \\ \vdots \\ \Delta z \end{bmatrix} \quad (1) $$

in which $[\mathbf{R}]$ is a 3×3 rotation matrix that orients the C-frame relative to the ℓ-frame, $[\emptyset_3]$ is the 3×3 null matrix, and $[\mathbf{X}]$ is the skew symmetric matrix

$$ {}^{\ell}[\mathbf{X}] = \begin{bmatrix} 0 & -c_z & c_y \\ c_z & 0 & -c_x \\ -c_y & c_x & 0 \end{bmatrix} \quad (2) $$

that represents the components of a vector $\vec{\mathbf{c}}$ that points *from* the origin of the ℓ-frame *to* the origin of the C-frame. For the convenience of the reader, the pre-superscripts identify the reference ℓ-frame in which the elements of a matrix are measured. To our knowledge the first use of the transformation in Eq. (1) was by Yuan and Freudenstein [17] for kinematic representations of mechanisms, but it also was derived independently by Bourdet and Clément [9] to transfer SDT coordinates for a measured feature from one coordinate frame to another. They called it the *transfer matrix*.

Since intersecting half-spaces is more easily accomplished with the dual coordinates of hyperplanes [18,19] instead of SDT coordinates, we here adapt Eq. (1) to transform directly hyperplane coordinates in dimension 6. Just as in dimension 3 [12], we find that the *inverse* of the kinematic transformation is required to transform coordinates of a plane (hyperplane in higher dimensions).

Using homogeneous point- or plane-coordinates,

$$\left[a_\phi \cdots a_{\Delta z}\; b\right]\;[\phi \cdots \Delta z\; 1]^{\mathrm{T}} = 0 \tag{3}$$

represents a hyperplane [18] in 6D *homogeneous* SDT point-coordinates $(\phi, \cdots, \Delta z, 1) = (\phi, \psi, \theta, \Delta x, \Delta y, \Delta z, 1)$ or in homogeneous plane-coordinates $(a_\phi, \cdots, a_{\Delta z}, b) = (a_\phi, a_\psi, a_\theta, a_{\Delta x}, a_{\Delta y}, a_{\Delta z}, b)$. The directed normal distance *from* the plane *to* the origin of the reference frame is $b/\sqrt{\sum a_k^2}$. With the positive sign on the square root, the directed sense is consistent with that of the vector $(a_\phi, \cdots, a_{\Delta z})$ [12,18]. Note that a set of coordinates $(a_\phi, \cdots, a_{\Delta z}, b)$ for a plane also represents a half-space because all points giving a positive non-zero product in Eq. (3) lie on one side of the plane (Ch. 4 in [12]).

For *homogeneous* coordinates $(\phi, \cdots, \Delta z, 1)$ of a SDT (a point in 6D), Eq. (1) may be applied using [16]

$$^{\ell}\begin{bmatrix}\phi\\ \psi\\ \theta\\ \Delta x\\ \Delta y\\ \Delta z\\ 1\end{bmatrix} = {}^{\ell}\begin{bmatrix} & & & & & & 0\\ & [\mathbf{R}] & & & [\emptyset_3] & & 0\\ & & & & & & 0\\ & & & & & & 0\\ & [\mathbf{X}][\mathbf{R}] & & & [\mathbf{R}] & & 0\\ & & & & & & 0\\ 0 & 0 & 0 & 0 & 0 & 0 & 1\end{bmatrix} {}^{C}\begin{bmatrix}\phi\\ \psi\\ \theta\\ \Delta x\\ \Delta y\\ \Delta z\\ 1\end{bmatrix} \equiv {}^{\ell}[\$\$\$]\; {}^{C}\begin{bmatrix}\phi\\ \psi\\ \theta\\ \Delta x\\ \Delta y\\ \Delta z\\ 1\end{bmatrix}. \tag{4}$$

Since Eq. (3) must hold in any reference frame, and since, for two frames ℓ and C, the T-Map point is transformed with Eq. (4), mathematical consistency requires that Eq. (3) be written

$$^{C}\left[a_\phi \cdots a_{\Delta z}\; b\right] {}^{\ell}[\$\$\$]^{-1}\; {}^{\ell}[\$\$\$]\; {}^{C}[\phi \cdots \Delta z\; 1]^{\mathrm{T}} = 0\,. \tag{5}$$

Consequently, the kinematic transformation for hyperplane coordinates in 6D is

$$^{\ell}\left[a_\phi \cdots a_{\Delta z}\; b\right] = {}^{C}\left[a_\phi \cdots a_{\Delta z}\; b\right] {}^{\ell}[\$\$\$]^{-1}\;, \tag{6}$$

in which ${}^{\ell}[\$\$\$]^{-1}$ is formed with the same seventh row and column as ${}^{\ell}[\$\$\$]$, but the upper left six-by-six submatrix ${}^{\ell}[\$\$]$ (Eq. (4)) is replaced with [16]

$$^{\ell}[\$\$]^{-1} = {}^{\ell}\begin{bmatrix}[\mathbf{R}]^{\mathrm{T}} & [\emptyset_3]\\ \left[[\mathbf{X}][\mathbf{R}]\right]^{\mathrm{T}} & [\mathbf{R}]^{\mathrm{T}}\end{bmatrix}. \tag{7}$$

5. The part-level T-Map for a circular pattern of four cylinders

The construction of T-Maps for a pattern of holes or pins with half-spaces may be decomposed into the following steps:

i) Produce the generic T-Map primitive for each constraint in its own generic C-frame of reference,
ii) With the inverse kinematic transformation, represent each of these in the canonical reference frame for the entire pattern, which provides the greatest symmetry, and
iii) Intersect all the transformed T-Map primitives to form the T-Map for the entire pattern in the canonical frame.

In this section the steps will be illustrated with a circular pattern of four holes. Examples of other patterns are in §6.

5.1. The generic T-Map primitive at one constraint circle

The constraint circle C in Fig. 2(b) is reproduced in Fig. 3(a), now shown approximated with 8 lines tangent to it. The $x_C y_C z_C$-frame shown is 3D, and it is attached to the tolerance-zone. In the 6D co-domain point-space of the T-Map or deviation space, each line represents a half-space with an inward-directed normal vector, so capturing all the points in the circle (and a small amount more). Since the boundary constraints provided to each half-space by circle C are only SDT coordinates Δx and Δy, the other coordinates ϕ, ψ, θ, and Δz are unbounded. Taking each unbounded one in turn, e.g. θ, the generic T-Map shape is a right circular cylinder in the $\theta\Delta x\Delta y$-frame. These cylinders are shown in Fig. 3(b) for all four unbounded SDT coordinates.

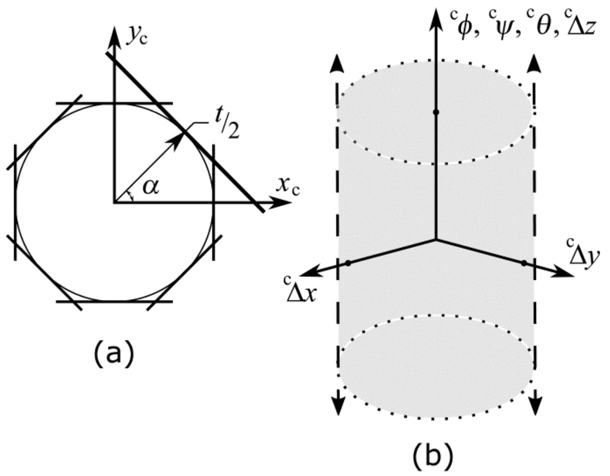

Fig. 3. (a) constraint circle C approximated by tangent half-spaces; (b) the corresponding bounded shape in SDT coordinates.

5.2. Transforming generic T-Map primitives

Since the only constrained coordinates $(a_\phi, \cdots, a_{\Delta z}, b)$ in the $x_C y_C z_C$-frame are Δx and Δy for each hyperplane in Fig. 3(a), the required set of coordinates at the right in Eq. (6) may be written ${}^{C}[0\;\;0\;\;0\;\; -\cos\alpha\;\; -\sin\alpha\;\; 0\;\; t/2]$, $0 \le \alpha < 2\pi$. There are three consequences of our assumption (§2) that the mating planes between Parts 1 and 2 just control SDT coordinates ϕ, ψ, and Δz. First, the half-space coordinates at the left in Eq. (6) for the pattern may be written ${}^{\ell}[0\;\;0\;\; a_\theta\;\; -\cos\alpha\;\; -\sin\alpha\;\; 0\;\; t/2]$; these correspond to the canonical xyz-frame in Fig. 2(a). Second, a reduced inverse kinematic transformation

$$^{c}[\,0, -\cos\alpha\,, -\sin\alpha\,, t/2]\;\, {}^{\ell}\begin{bmatrix} 1 & 0 & 0 & 0 \\ -c_y & 1 & 0 & 0 \\ c_x & 0 & 1 & 0 \\ 0 & 0 & 0 & 1 \end{bmatrix} \tag{8}$$

for half-spaces may be used to obtain $^{\ell}[\,a_\theta \;\; a_{\Delta\mathrm{x}} \;\; a_{\Delta\mathrm{y}} \;\; b\,]$, where the matrix in Eq. (8) is obtained from $^{\ell}[\$\$\$]^{-1}$ by striking out the first, second, and sixth columns and rows. Third, the orientations of the cylinder axes do not control rotations ϕ and ψ at the part level, so the coordinate c_z of vector $\vec{\mathbf{c}}$ is unimportant and is ignored. Further, with c_z ignored, the same half-spaces are generated from an upper constraint circle $\overline{C}$ (Fig. 2(b)) as are generated from the corresponding lower constraint circle C. (However, note that, when using half-spaces to generate the T-Map for an *single axis* (e.g. for a hole), the result is very different [13,16]: (a) the tolerance-zone then *controls* SDT coordinates ϕ, and ψ, (b) the origin of the local frame (ℓ) is mid-way along the depth of the hole, and (c) component c_z of vector $\vec{\mathbf{c}}$ *must* be used— $+c_z$ for circle $\overline{C}$ and $-c_z$ for circle C.)

The transformation in Eq. (8) shears the half-spaces parallel to the $\Delta x\Delta y$-plane of the T-Map, but it modifies only half-space coordinate a_θ which, in general, becomes

$$^{\ell}a_\theta = \left(c_y \cos\alpha - c_x \sin\alpha\right). \tag{9}$$

As one example of transformation, take the half-space represented with $\alpha = 45^{\circ}$ (the wider tangent line in Fig. 3(a)). When this halfspace is tangent to a constraint circle at either the hole in the second or the fourth quadrants of the xyz-frame of Fig. 2(a), $^{\ell}a_\theta = \pm d/2$, respectively, where d is the diameter of the circular pattern. When the 45°-half-space is tangent to a circle at either the hole in the first or the third quadrants, $^{\ell}a_\theta = 0$, the half-space remains parallel to the θ-axis, and it is redundant in the intersection.

5.3. Part-level T-Map by intersecting transformed primitives

To give better resolution to the finished T-Maps here and in §6, we replace the circumscribing octagon in Fig. 3(a) with a 40-sided regular polygon. After every generic T-Map primitive has been transformed so that its translational coordinates correspond to the canonical, or local, ℓxyz-frame (xyz-frame in Fig. 2(a)), all 8 constraint circles coincide, and multiple half-spaces pass through each of the 40 tangent lines. The finished T-Map in Fig. 4 is formed by intersecting them using *qhull* [20], an open source C++ library. The diameter of the circle is tolerance t that transfers from Figs. 2 and 3(a).

Continuing further the example of §5.2, for the 45°- half-space that is tangent to the fourth-quadrant hole, Eq. (3) gives $-(d/2)\theta - \Delta x/\sqrt{2} - \Delta y/\sqrt{2} + t/2 = 0$ in the ℓ-frame. The three SDT axes pierce this half-space at $\theta = t/d$ and $\Delta x = \Delta y = t/\sqrt{2}$ [12]. Therefore, to maximize the symmetry of the T-Map shown in Fig. 4 for the ℓ-frame, we use a characteristic length of $d/2$ to change the scale and dimension (to length [L]) of the SDT θ-coordinate. The new coordinate is $\theta' = \theta\, d/2$, and its intercept with the 45°- half-space is $t/2$.

For the maximum material condition (MMC) specification Ⓜ in Fig. 1, the T-Maps in Fig. 4 may be bigger or smaller,

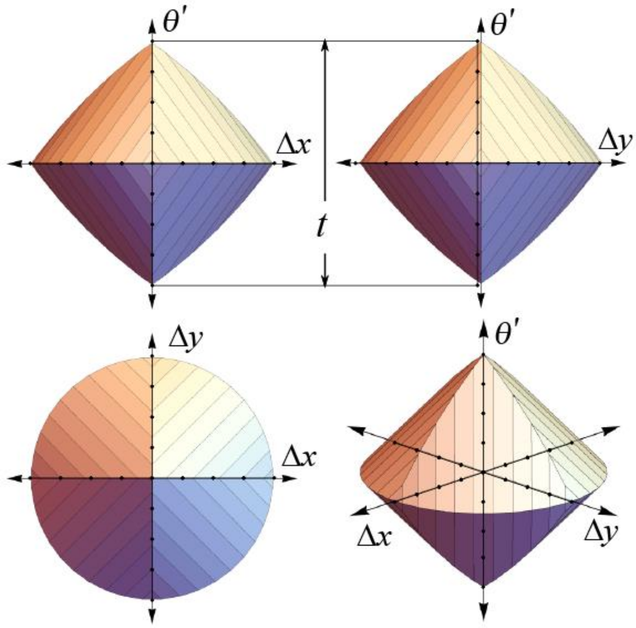

Fig. 4. Part-level T-Map for a circular (square) pattern of four holes.

according to the manufactured size of the controlling holes. When the two parts in Fig. 2(c) are assembled and the pins in Part 1 are perfectly positioned and of virtual condition size (a gage) the diameter of the T-Map circle in Fig. 4, and also the constraint circle in Fig. 3(a), ranges from $t = 2t_h$ to $t = 2(t_h + \tau_h)$, where t_h and τ_h are the position and size tolerances for the holes (0.1 mm and 0.2 mm, respectively, in Fig. 1). Of course, for worst-case tolerance analysis, the largest T-Maps in Fig. 4 should be used, i.e. for $t = 2(t_h + \tau_h)$.

Note that each of the four pairs of opposite surfaces in Fig. 4 derives from one circle of constraint. In contradiction to the recommendation in §5.2, the component c_z of vector $\vec{\mathbf{c}}$ may be retained for transformation of T-Map primitives from all eight constraint circles in Fig 2(a). Then, after intersection, all of the surfaces produced are doubly traced. The surfaces from two constraint circles i and j for which the vectors $\vec{\mathbf{c}}_i = -\vec{\mathbf{c}}_j$ generate the same pair of surfaces in Fig. 4.

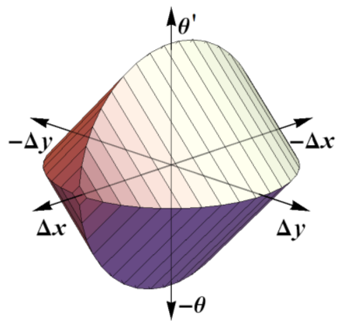

Fig. 5. Part-level T-Map for two opposite holes, e.g. a pair from Fig. 2.

A validation of the method may be made by intersecting only those half-spaces for one opposite pair of holes in Fig. 2(a). This result is in Fig. 5 and is the same as that obtained for a linear pattern of holes in [2, Fig. 11(a)]. Note that, to be consistent with [2], Fig. 5 was constructed for an $x'y'$-frame having one axis on the line joining the two circles. This required the matrix in Eq. (8) to include a 45° rotation [**R**] from Eq. (7).

For n tangents around each constraint circle in Fig. 3, the computational complexity is O(n^2). Although the time of computation is also a function of the computer used, we found that computations to generate and transform the T-Map for one hole was 0.016 sec for 8 tangents, and 0.26 sec for 40 tangents. The time to compute the T-Map for any four-hole pattern, such as the one shown in Fig. 4, was 3.0 sec.

6. Part-level T-Maps for other patterns of pins or holes

Two other example patterns of four holes are shown in Fig 6: rectangular and irregular. To make the corresponding T-Maps comparable to those in Figs. 4 and 5, dimension a is 20 mm (Fig. 1) and the characteristic length remains $10\sqrt{2}$ mm. The T-Maps are shown in Figs. 7 and 8. For worst-case analysis, the diameters of the circles are the same as before, i.e. $t = t_h + \tau_h$. However, for the irregular pattern in Fig. 6(b), the origin of the local (ℓ) frame is located at the mid-span of the line joining the furthest separated pair of holes.

One consequence of retaining the same characteristic length is that the T-Map for the rectangular pattern of holes in Fig. 7 has a reduced peak-to-peak span along the θ'-axis from that for the square pattern (Fig. 4). The ratio of diagonal for the a×a sized square to diagonal for the a×$2a$ sized rectangle equals $(1/\sqrt{5})$ which is the scaling factor shown in Fig. 7.

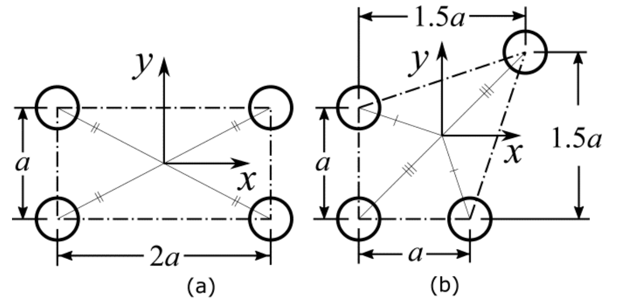

Fig. 6. (a) rectangular pattern of holes; (b) irregular pattern.

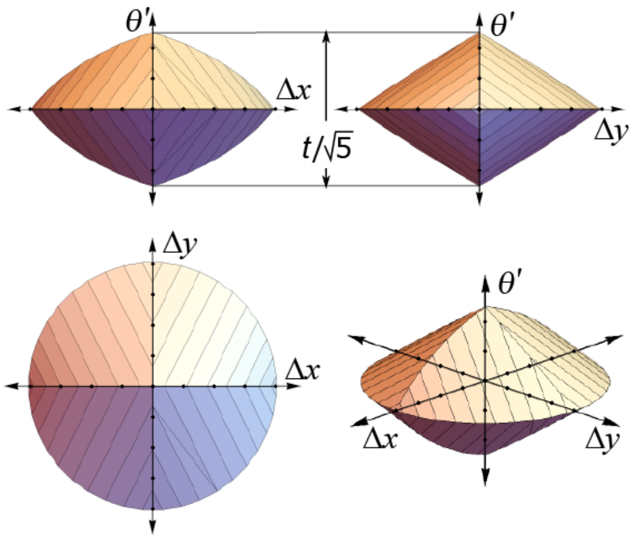

Fig. 7. Part-level T-Map for the rectangular pattern of holes in Fig. 5(a)..

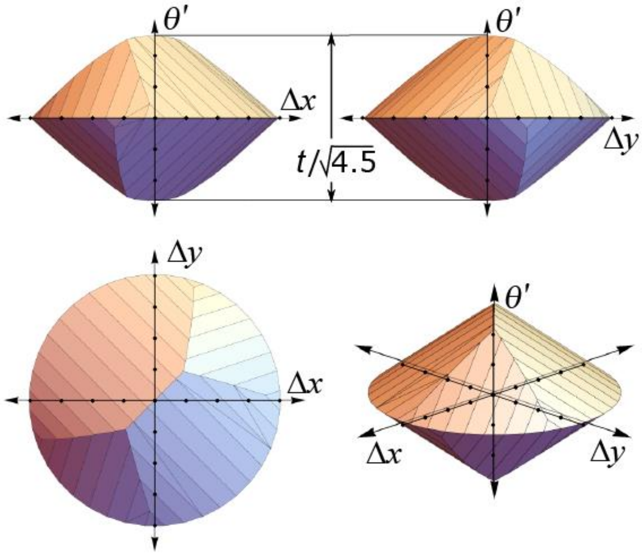

Fig. 8. Part-level T-Map for the irregular pattern of holes in Fig. 5(b).

Similarly, the ratio of diagonal of the a×a sized square to diagonal for a $1.5a$-by-$1.5a$ sized rectangle is $(1/\sqrt{4.5})$ which is the scaling factor shown in Fig. 8.

The upper half of the T-Map boundary in Fig. 8 is formed from four curved surfaces that are separated by five edges. Of these four surfaces, the two opposite ones with smaller area are formed from the opposite pair of holes nearer to the origin in Fig. 6(b). The two surfaces with larger area are formed from the furthest separated opposite pair of holes.

7. Patterns of many holes

The T-Map for a pattern of two holes is the Archimedean globe [21] in Fig. 5. As the number of holes in a circular pattern increases, each opposite pair yields the same Archimedean shape, but now rotated about the θ'-axis an amount from the first globe. All of these Archimedean globes, each rotated somewhat from the others, are intersected to form the T-Map for the entire circular pattern. As the number of holes increases, the limiting shape is a dicone for the T-Map. Further, so long as the origin of the local (ℓ) frame is at the mid-span of the furthest separated pair of holes (or pins) in the pattern (e.g. in Fig. 6(b)), maximum symmetry is achieved: the T-Map is a *right* dicone, and a simpler method can be used for its construction, so reducing the time of computation.

8. Part-level T-Map for tolerances on the patterns of both pins and holes

When size and position tolerances for the pins in Part 1 are also included in the model for the assembly of Fig. 2(c), the T-Maps in Figs. 4, 5, 7, and 8 are larger, but unchanged in shape. For worst-case tolerance descriptions, the diameters of the circles, and dimension T, are now $t = 2(t_h + \tau_h + t_p + \tau_p)$ where t_p and τ_p are the position and size tolerances for the pins and the MMC specification prevails for the pins also. When the minimum radial clearance c_{min} is greater than zero in the assembly-level T-Map [2], $t = 2(t_h + \tau_h + c_{min} + t_p + \tau_p)$. These T-

Maps for fully toleranced assemblies of Parts 1 and 2 (Fig. 2(c)) also may be regarded as formed from Minkowsi sums of three geometrically similar T-Maps: one for $t=2(t_h+\tau_h)$, one for $t=2c_{min}$, and one for $t=2(t_p+\tau_p)$. Note that the sums of tolerances, both here and in §5.3, are doubled. One sum is required to ensure clearance for assembly when Parts 1 and 2 in Fig. 2(c) are aligned to the same datums and there is no displacement between them. The other sum represents the full positional variation between the two parts when one is no longer aligned with the datums, but is instead free to move [22].

The coordinates Δx, Δy, and $\theta=2\theta'/d$ (Sect. 5.3) in Figs. 4, 7 and 8 represent, in terms of the tolerances specified for patterns of pins and holes, the largest SDT coordinates of displacement of the DRF ABC on Part 2 (Fig. 1) relative to a DRF on Part 1 (not shown). This physical significance of patterns is important in many assemblies, such as the array of holes for bolting together two halves of the casing for a centrifugal pump or the halves of a transmission housing. It is especially important when a shaft of the assembly is supported by two bearings, one in the housing component with threaded studs and the other in the component with holes.

9. Conclusion

The two principal contributions in this paper are: (1) Combine the constraints at several generic features of the tolerance-zones of a pattern of holes in a host part to form the T-Map that models allowable variations of the host part relative to another part that is assembled to it with a matching pattern of pins. (2) Utilize the kinematic transformation, which has been adapted to be used directly with higher-dimensional half-spaces, to transform every generic T-Map to a convenient local frame of reference for the entire pattern. By combining the size and position tolerances for the pins and holes that engage in an assembly, the T-Map may accommodate a material condition specification for either the holes or the pins or both. A minimum clearance may also be included.

Since the T-Maps in this paper are for an entire pattern of holes or pins, the entire pattern may be considered as a single feature in an assembly loop for tolerance analysis or synthesis.

Acknowledgements

The authors are grateful for funding provided to this project by Digital Manufacturing and Design Innovation Institute Grant #DMDII -16-01-02

References

[1] American National Standard ASME Y14.5M. *Dimensioning and Tolerancing*, New York: The American Society of Mechanical Engineers; 2009

[2] Ameta G, Singh G, Davidson JK, Shah JJ. Application of T-Maps for Composite Position Tolerance for Patterns of Features. In press for J. Comput. & Inf. Sci. Eng. 2018; #10.1115/1.4039473.

[3] International Organization for Standardization ISO 17450. Geometrical product specifications (GPS) - General concepts. ISO; 2011.

[4] Mujezinovič A, Davidson JK, Shah JJ. A new mathematical model for geometric tolerances as applied to polygonal faces. J. Mechanical Des. 2004; 126:504-18.

[5] He Y, Kalish N, Davidson JK, Shah JJ. Tolerance-Maps for line-profiles formed by intersecting kinematically transformed primitive T-Map elements. Accepted, J. Comput. & Inf. Sci. Eng. 2016; 16(2):021005.

[6] Giordano, M. Duret, D. Clearance Space and Deviation Space. 3rd CIRP Seminar on CAT 1993; Cachan, Fr, pp. 179-196. Paris: Eyrolles.

[7] Coxeter HSM. Introduction to geometry. 2nd ed. Toronto: Wiley; 1969.

[8] Cayley A. On the six coordinates of a line. Trans. of the Cambridge Phil. Soc. 1869; 11(II):290-323.

[9] Bourdet P, Clément A. Controlling a complex surface with a 3 axis measuring machine. Annals of the CIRP, Manufacturing Technology. 1976; 25(1):359-61.

[10] Bourdet P, Clément A. A study of optimal criteria identification based on the small displacement screw model. Annals of the CIRP 1988; 37: 503-6.

[11] Desrochers A, Ghie W, Lapérriere L. Application of a unified Jacobian-torsor model for tolerance analysis. J. Comput. & Inf. Sci. Eng. 2003; 3(1):2-14.

[12] Davidson JK, Hunt KH. Robots and screw theory: Applications of kinematics and statics to robotics. Oxford: OUP; 2004.

[13] Kalish N, Davidson J, Ramnath S, Haghighi P, Shah JJ, Shah, JV. Mathematical tools for automating digital fixture setups: constructing T-Maps and relating metrological data to coordinates for T-Maps and deviation spaces. In press for J. Comput. & Inf. Sci. Eng. 2018; #10.1115/1.4038821.

[14] Teissandier D, Contribution à l'Analyse des Tolerances Géométriques d'un Système Mécanique par des Polytopes. PhD Hab. Univ. Bordeaux 1; 2012.

[15] Arroyo-Tobón S, Teissandier D, Delos V. Tolerance Analysis with Polytopes in HV Description. J. Comput. Inf. Sci. Eng. 2017; 17(4): #10.1115/1.4036558.

[16] Kalish N. The theory behind Setup-Maps: a computational tool to position parts for machining. MS thesis. Arizona State University; 2016.

[17] Yuan, MSC, Freudenstein, F. Kinematic analysis of spatial mechanisms by means of screw coordinates–Part I. J. Eng. for Indus. 1971; 93B:61-6.

[18] Preparata FP, Shamos MI. Computational Geometry: An Introduction. New York:Springer-Verlag; 1985.

[19] Barber, CB, Dobkin, DP, Huhdanpaa, H. The Quickhull algorithm for convex hulls. ACM Trans. Math. Software 1996; 22(4):469-83.

[20] http://www.qhull.org

[21] Apostol, TM, Mnatsakanian, MA. New horizons in geometry. Wash., DC:Math Assoc. of Amer.; 2012.

[22] Singh, G, Ameta, G, Davidson, JK, Shah, JJ. Tolerance analysis and allocation of a self-aligning coupling assembly using Tolerance-Maps. J. Mechanical Des. 2013; 135:#10.1115/1.4023279.